Optomechanical design and fabrication of a wide field of view 250-mm-aperture freeform imaging system

Matthew A. Davies, Brian S. Dutterer, Steven Swagler, Eann Lawing, Nicholas Horvath[1]
Department of Mechanical Engineering and Engineering Science, The University of North Carolina at Charlotte, 9201 University City Boulevard, Charlotte NC, 28223, USA
(1)Currently at Lockheed Martin Corporation, Colorado, USA.
Jannick P. Rolland, Aaron Bauer
The Institute of Optics, University of Rochester, 275 Hutchison Rd, Rochester, NY 14627, USA

ABSTRACT

Freeform optics, containing optical surfaces with no axis of rotational invariance (within or beyond the optical part), introduce additional degrees of freedom into the optical design with a radical effect. We discuss the design and fabrication of two three-mirror-anastigma freeform telescopes using a concurrent engineering approach where optical designers, optical fabricators, metrologists, and optical testing experts are coordinated throughout the design process. While targeting large aperture systems, the design principles and results are first demonstrated with a 1/3rd scale system. A "snap-together" optical system was designed utilizing a multi-axis ultra-precision machine to manufacture the freeform optics and a monolithic optomechanical system. The advantage of the design was that it transferred machine accuracy into the final system and allowed for rapid assembly/disassembly (approximately 10 minutes for assembly). The disadvantage of the design was that there were no adjustments for recovery performance. Thus, the wavefront errors on this system were significant (approximately 1.25 micrometers), but the wavefront repeatability upon assembly/disassembly was only 25 nm. Sample imaging results are shown. The lessons learned from the smaller scale system we then applied to a large aperture system (260-mm). Interaction between the optical designers and the opto-mechanical designers and fabricators showed that the tolerances for the final system could be reduced substantially by combining the kinematic mounting design from the first system with minimal adjustment capability after assembly to recover performance. This finding considerably loosened the tolerances necessary for a detector-limited performance. It also allowed the use of less expensive aerospace precision machine tools to manufacture the housing components, while the more expensive ultra-precision diamond machining equipment could be used to produce the freeform optical surfaces. Off-the-shelf positioning stages are used for the system adjustments leading to an overall lower cost for the system. Details of the manufacture and metrology of the optomechanical system, the freeform optics, and the plans for system testing are discussed. A large freeform mirror (the system secondary) 120 mm in diameter is manufactured, and the errors are below one micrometer. These errors are being evaluated for the final system before the final mirrors are completed.

1. INTRODUCTION

Freeform optics, containing optical surfaces with no axis of rotational invariance (within or beyond the optical part), introduce additional degrees of freedom into the optical design with a radical effect [1]. Freeform optics are proving to be a disruptive technology that is leading to the re-engineering of optical designs across industry with applications from infrared imaging, virtual and augmented reality systems, cameras, microscope and telescope systems, etc. Freeform optics allow reduced size and weight, improved performance, reduced system cost, improved manufacturability, and often entirely new optical functionality [2,3]. For imaging and surveillance, wide-field of view, large aperture, and unobstructed systems with optimization of aberrations over the full field of view are possible using freeform systems. However, judicious choice of starting geometry in the optical design is critical to maintaining feasibility and control costs [4,5]. Further, to realize the benefits of freeform optics in the final physical imaging systems requires a concurrent engineering approach where optical design, fabrication, metrology, opto-mechanics, and desired field performance are considered simultaneously [6,7]. A concurrent approach can have a radical impact on system cost and performance.

Freeform optics introduce an infinite number of degrees of freedom in the optical and the opto-mechanical design. Additionally, unlike traditional on-axis, symmetric designs, freeform optical systems require that the optics be located precisely in all six degrees of freedom. For example, in an axisymmetric design with axisymmetric optics, clocking

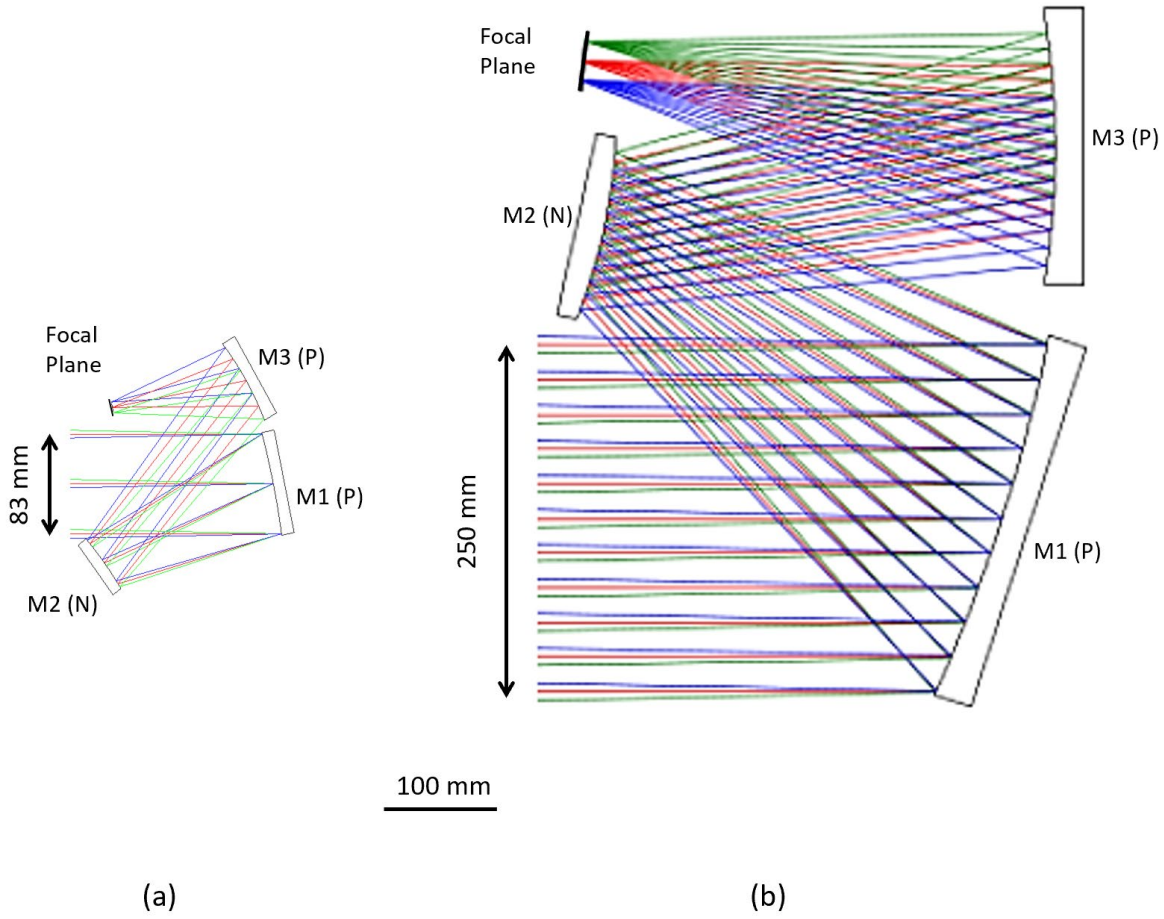

Fig. 1. Two three-mirror, in plane, freeform optical designs, both with a positive-negative-positive (i.e. concave-convex-concave) layout with (a) having an 83 mm aperture and (b) having a 250 mm aperture.

(rotation about the axis of symmetry, usually the optical axis) is not an important degree of freedom, whereas with a freeform surface, it can be critical. If a serial assembly approach is adopted, there is significant complexity in aligning each subsequent optic with six degrees of freedom relative to the previous optic with sufficient accuracy to achieve overall system performance goals. In our work, we have adopted a different approach. The system is engineered concurrently, so form tolerances, position and assembly tolerances, and optical adjustment for recovering performance are considered simultaneously. The capabilities of manufacturing and metrology systems are also considered in the design process to optimize the end result. Fiducials for metrology and mechanical alignment features are manufactured in the same setup as that used for the manufacturing of the freeform optical surfaces, transferring machine accuracy into the surface. The metrology and alignment features were demonstrated by Horvath et al. [8]. In addition, kinematic mounting/alignment features such as a three-ball three-vee design can produce an in-plane position uncertainty of less than 200 nm, an axial positioning uncertainty of 40 nm, and an angular positioning uncertainty of less than 1 microradian in all three angular degrees of freedom [9].

Precision engineering principles such as kinematic mounting systems are coupled with freeform optical system design, and the results are demonstrated in this paper for two freeform optical systems. The first system is a smaller scale demonstrator, a three-mirror freeform, 83 mm aperture, imager operating at F/3 over a 1°×1° full FOV. While not the ideal optical design, this system was used to develop optical design and manufacturing methods for larger systems. The second system described in this paper is a three mirror anastigmat (TMA) off-axis in-plane optical design. The system is 250 mm aperture-class three-mirror imager operating at F/3 over a 2.12° by 2.12° full FOV, with diffraction-limited performance (optical design) over the visible spectrum for a system volume of about 72 liters, a target mass of 15 kg, and a 36.4 mm by 27.6 mm detector with 4.6 μm pixel spacing.

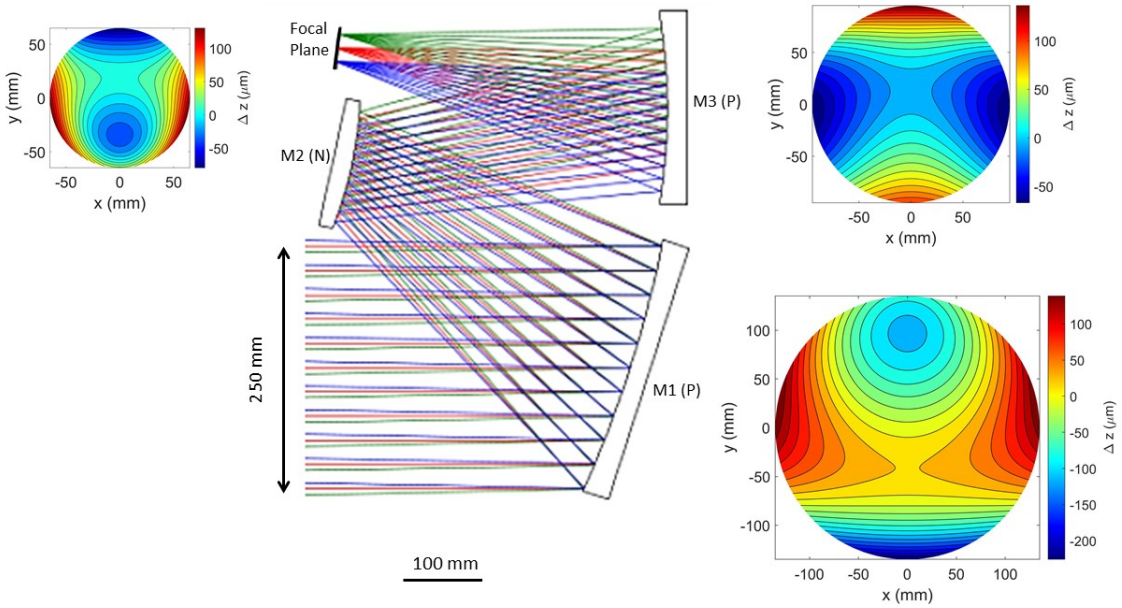

Fig. 2. Design shown in Fig. 1(b). The overall form of the mirrors is concave (positive), convex (negative) and positive (concave), the freeform departure of each mirror is shown.

Both of these designs are prototyped in metal. The housings are manufactured with conventional precision machining. The optical surfaces are manufactured using ultra-precision diamond machining. In the first design, a monolithic housing was used. In the second, precision linear adjustments of one mirror are introduced to make the tolerances more attainable. The challenges and benefits of both approaches are compared and contrasted.

2. FREEFORM OPTICAL DESIGNS: FABRICATION AND MEASUREMENT CHALLENGES

The two optical designs examined in this paper are shown in Fig. 1. Both have a positive primary mirror (M1), a negative secondary mirror (M2), and a positive tertiary mirror (M3) before the light is focused on the focal plane. The topographical layout of the systems is different, and the details of the methods for choosing an optimum freeform geometry are given in Bauer et al. [5]. However, from the optomechanical and fabrication standpoint, the two designs present similar challenges. Each has three freeform mirrors that must be positioned in space relative to the other mirrors and the focal plane (detector) with six degrees of freedom. The optical design principles used to generate three-mirror wide fields of view systems of this type with diffraction-limited performance are reported by Bauer et al. [6, 10].

To understand the fabrication and assembly challenges further, refer to Fig 2., which shows the larger design (Fig 1(b)) with the deviation from the aspheric component (freeform deviation Δz) overlaid on the system layout. Mirror M1 has an overall sagittal depth of approximately 8 mm and a freeform deviation of 383 micrometers. Mirror M2 has an overall sagittal depth of approximately 5 mm and a freeform deviation of 220 micrometers. Mirror M3 has an overall sagittal depth of approximately 8 mm and a freeform deviation of 214 micrometers. Thus, while the freeforms are dominantly symmetric, they have a significant freeform component as well (hundreds of micrometers).

Symmetric but non-spherical optics (aspheres) are most often fabricated using ultraprecision computer numerical controlled (CNC) manufacturing systems. As described by Thompson and Rolland, ultraprecision diamond turning was an enabling technology for aspheric optics and optical system designs [1]. Technology for the modern diamond turning machine initially developed in industry in the early 1900s [11,12]. It accelerated in the US weapons

Fig. 3. Two diamond machining centers (a) a Moore Nanotechnology 350 FG and (b) a Moore Nanotechnology 650 FG with five degrees of freedom, three linear axes (X,Y,Z) and two rotational axes (C, B) used in (c) a coordinated axis turning configuration.

laboratories and industrial partners in the latter half of the 20th Century [13-16]. With this technology, a single-crystal diamond tool was used with an ultraprecision lathe typically having air-bearing spindles and two linear hydrostatic slides with interferometric position feedback (typically the X and Z axes with X perpendicular to the spindle axis and Z parallel to the spindle axis). The initial technology was limited to two degrees of freedom. This allowed for the manufacturing of aspheric surfaces, including off-axis parabolic surfaces. However, to manufacture a freeform surface such as those shown in Fig. 2 required at least one additional degree of freedom. The additional degree of freedom was initially implemented with the fast tool servo system, where the tool could be moved parallel to the spindle axis (ΔZ) in coordination with the angle (C) of the spindle axis [17]. Further development of the technology led to diamond machining centers with five or more degrees of freedom, and it is this technology that has become a primary enabler for freeform optics [4]. The work reported here was completed on two five-axis machining centers, a Moore Nanotechnology 350 FG and a modern Moore Nanotechnology 650 FG diamond machining center as shown in Fig.e 3. The optics for the small-scale design (Fig. 1(a)) were machined on the Moore 350 FG machine. The optics for the large-scale system (Fig. 1(b)) are being machined on the Moore 650 FG machine. In each case, the machines are being used in coordinated axis machining mode where the three degrees of freedom to generate the freeform surface are X, Z, and C.

3. SMALL SCALE PROTOTYPE

Detailed development of this prototype is described by Horvath et al. [8]. We summarize these results here to give context for the modifications of the design made on the large-scale design. The tolerances dictated by sensitivity analysis on the optical design are given in Table 1, column 2, and the expected uncertainties with the manufacturing methods described below are in column 3.

Table 1: Tolerances for small-scale freeform prototype.

Motion	Tolerance	Target Uncertainty
In-plane position (x/y in μm)	14	5
Optical axis (z in μm)	9	3
Clocking (μrad)	141	28
Tip/Tilt (μrad)	86	17

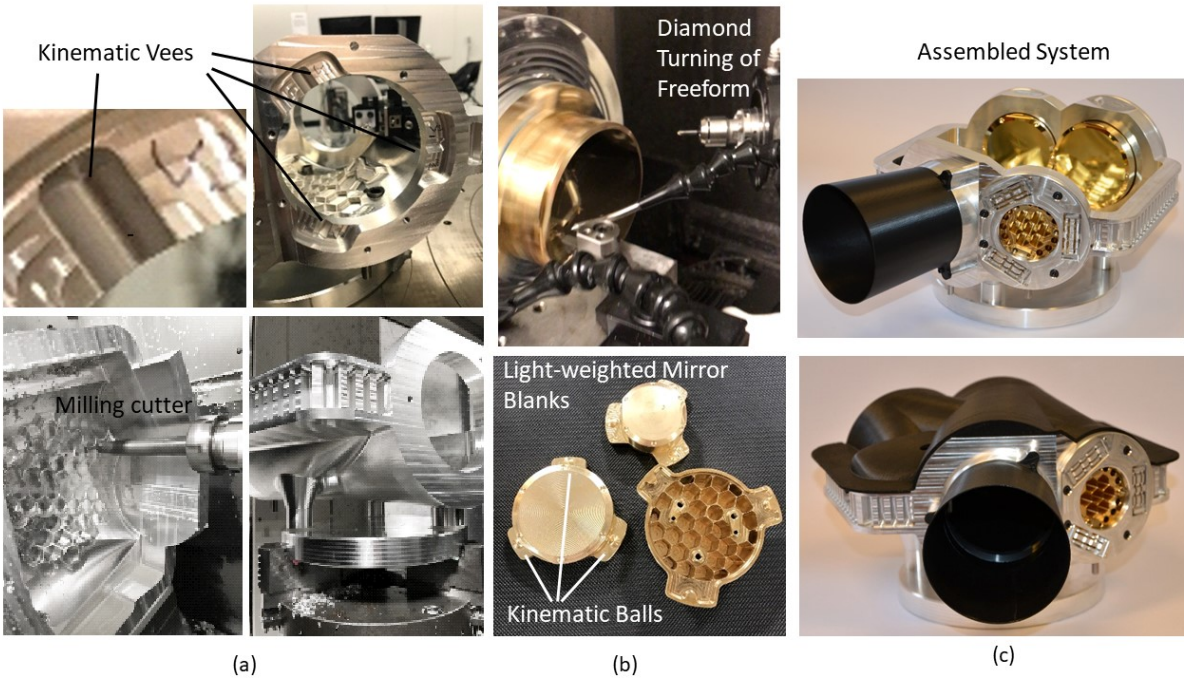

Fig 4. Monolithic three-mirror freeform telescope prototype showing manufacture of (a) monolithic aluminum housing with kinematic vee features, (b) mirror blanks and mirror with kinematic ball features, and (c) final assembled system,

Because the system is open/unobstructed with the three mirrors placed around a periphery (Fig. 1(a)), the design included a monolithic housing and three monolithic mirrors that mated together with three-ball, three-vee kinematic mounts. The mirrors had no build-in adjustments, and therefore the uncertainties had to be controlled in the manufacturing machines methods and procedures. The advantage of this design is that it is "snap-together" and can be disassembled and reassembled in approximately 10 minutes.

The mechanical frame was machined from solid aluminum 7075-T6 on a Makino A55 high-speed precision machining center with a 20,000 rpm spindle and 0.6 m/s maximum slide speeds. This machine is capable of removing approximately 2500 cubic centimeters of aluminum in one minute and has the accuracies required to meet the target uncertainties. Three V-grooves, spaced equally 120° apart, were machined for each of the three optics around the periphery of the housing. The optics were also monolithic, with the mounting features, optical surfaces, and metrology fiducials all made in one machine setup. The manufacture of the housing is shown in Figure 4(a).

The mirrors were manufactured from C464 Naval brass, a durable but "diamond turnable" metal. The mirrors were mated with the housing using three-ball/three-vee kinematic mounts to meet the positioning uncertainties. The optics were made from C464 Naval brass and were light-weighted with a hexagon structure so that the face sheet thickness was 1.5 mm and the web thickness was 0.4 mm, as shown in Fig 4(b). The optical surfaces were manufactured by coordinated axis diamond machining on the Moore 350 FG machine. These surfaces had a maximum freeform departure of 590 μm and the surface irregularity tolerances were less than 0.5 μm.

Fig 5. Example images from the prototype system.

Table 2: Tolerances for large scale system with M2 compensator.

Diffraction Limited Performance			
Motion	M1	M2	M3
X/Y Decenter (μm)	100	Compensator	100
Z Despace (μm)	100	Compensator	100
Tip/Tilt (μrad)	100	100	100
Clocking (μrad)	200	200	200
Irregularity (PV) (μm)	0.3	0.3	0.3
Power (Fringes)	3	3	3

The optical surfaces and the kinematic balls were machined in the same setup as the kinematic balls to reduce the uncertainty in surface location relative to the kinematic features to less than 1 μm. These manufacturing steps should have allowed us to reach the position tolerances in Table 1. However, due to the lack of adequate metrology tools available at the time (5 years ago) the figure error on the freeform optical surfaces could not be verified.

Example images from the system are shown in Fig. 5. While this qualitative result was promising, subsequent wavefront testing indicated a total wavefront error of approximately 1.25 μm which made the system far from diffraction-limited. However, repeated wavefront testing upon assembly and disassembly showed that the wavefront repeatability was approximately 25 nm. The likely source of the wavefront errors was in the mirror form but the metrology was not available to diagnose the problem. However, the wavefront repeatability showed that the three-ball, three-vee kinematic mounts were highly repeatable. These lessons were taken into the larger system design.

4. LARGE SCALE SYSTEM DESIGN AND FABRICATION

Based on the results from the small scale prototype, several changes were made in the large scale system design: (1) three-ball, three-vee kinematic mounts were retained for repeatability but x-y-z adjustment was allowed for mirror 2 to allow for performance recovery and less stringent tolerances, (2) metrology was developed on the machine (Moore 650FG) to check mirror form before independent metrology and testing, (3) tolerances were developed for both diffraction-limited and detector-limited performance, (4) realizable metrology datums were added to the mirrors, (5) only the portion of the housing where M1 and M3 were mounted was made monolithic, (6) kinematic mounts were made for the machine and the metrology equipment that matched the three-vee mount on the housing so that mirrors were machined in the same state as they will be used. These changes were the result of the development of a truly concurrent engineering approach where optical designers, optical fabricators, opto-mechanical designers, and metrologists all had input into the design with several design reviews.

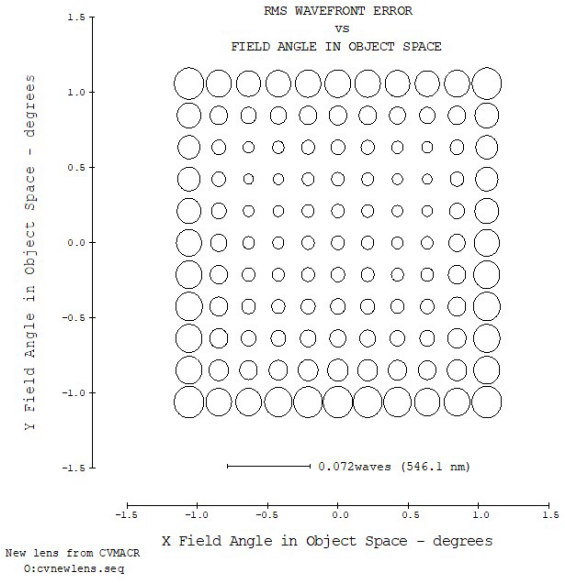

Fig 6. Full-field display of RMS wavefront error map of system shown in Fig 1(b) showing diffraction limited (< 0.072 waves) at 546.1 nm.

4.1 Nominal and Detector-Limited Optical Performance

To quantify system tolerances, achievable optical performance targets were defined. The optical system as-designed is diffraction limited at 546.1 nm over the 2.12° × 2.12° full FOV as shown in the root mean squared wavefront error full field display (FFD) shown in Fig. 6 (see [5] for the details of the

Table 3: Tolerances for large scale system with M2 compensator.

Detector Limited Performance			
Motion	M1	M2	M3
X/Y Decenter (μm)	500	Compensator	500
Z Despace (μm)	500	Compensator	500
Tip/Tilt (μrad)	460	540	1200
Clocking (μrad)	1900	1950	4100
Irregularity (PV) (μm)	0.75	0.75	0.75
Power (Fringes)	5	5	5

Table 4: Revised tolerances for large scale system with M2 compensator and tighter mirror location tolerances.

Detector Limited Performance (Modifed)			
Motion	M1	M2	M3
X/Y Decenter (μm)	250	Compensator	250
Z Despace (μm)	250	Compensator	250
Tip/Tilt (μrad)	230	230	230
Clocking (μrad)	950	950	950
Irregularity (PV) (μm)	1 (2)	0.46 (0.92)	0.70 (1.41)
Power (Fringes)	5	5	5

systematic design process). The angular diffraction limit of the system is given by Eq. (1) as

$$\Delta\alpha = 1.22\frac{\lambda}{D}\ , \tag{1}$$

where λ is the operational wavelength (546.1 nm), D is the aperture (260 mm), and $\Delta\alpha$ is the angular diffraction limit equal to 2.7 μrad. The effective focal length of the system is 750 mm; thus the diffraction-limited resolution on the detector plane is 1.9 μm over a 27.72 mm detector. However, the detector available for the system is 36.4 mm by 27.6 mm (7920x6004 pixels) with 4.6 µm pixel pitch (Emergent Technologies HT-50000). The final system will be detector-limited with this current detector and targeting detector limited performance significantly changes the tolerances and hence the opto-mechanical design.

4.2 System Tolerances

Because of the difficulties meeting the tolerances in the monolithic system, it was first decided to allow for limited adjustment of the system to enable performance recovery and relieve some of the tight tolerance constraints. In the optical design, it was found that three linear degrees of freedom on mirror M2 allowed for a significant increase in the tolerance limits. Further, it was determined that the adjustment resolution was attainable with a commercially available precision positioning stage: x-y-z linear stage with a travel of 12.7 mm, crossed roller bearing, angular deviation < 100 μrad, manual drive with micrometer screws, 1 μm fine revolution, sensitive 0.1 μm, lockable, upgradable to motorized adjustment. Defocus adjustment is also possible with a lower precision stage.

The tolerances needed for diffraction limited performance are given in Table 2. The tolerances on this system with the compensator are less stringent than those for the monolithic system because of the compensator and the possible recovery performance. However, on a system this large, particularly with the large mirrors, 300 nm of irregularity is challenging to produce by diamond machining. It is also difficult to measure the irregularity without moving to a high-cost solution such as a computer-generated hologram (CGH).

Because the system will be detector-limited, that performance was targeted and the associated more practical tolerances are given in Table 3. These are significantly less stringent than those in Table 2. In particular, the tolerances

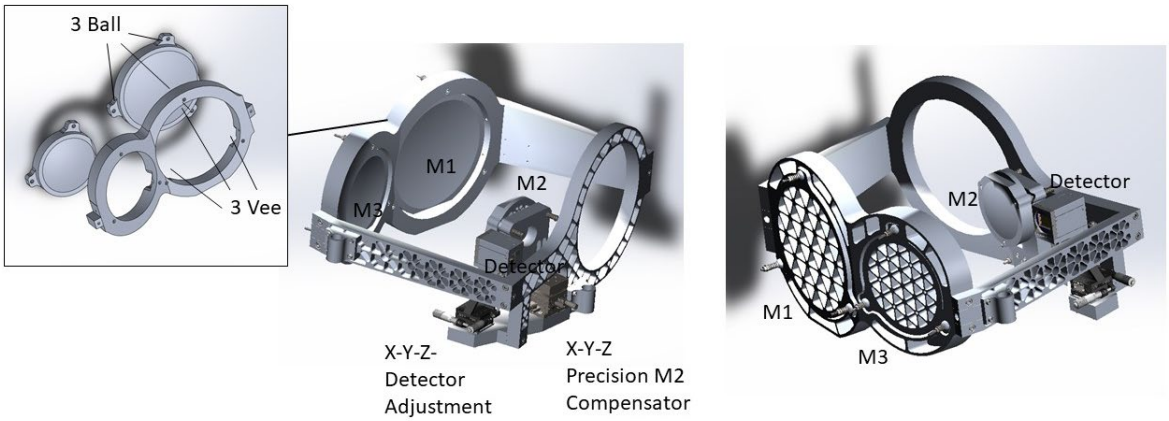

Fig 7. Opto-mechanical design of large scale system with the optical design shown in Fig. 1(b) and Fig. 2.

on mirror location and orientation are an order of magnitude less stringent than those for the original monolithic prototype system. However, the tolerances of 750 nm on mirror irregularity are still tight. Then an important concurrent engineering question was asked – if we can tighten the tolerances on mirror positioning by a factor of two using a precision machine (Makino A51), could the irregularity tolerance be made less stringent? Also, it was noted that due to thermal and machine errors, the irregularity of the mirrors will roughly scale with the mirror clear aperture. Answering this question resulted in the final tolerances given in Table 4, where we note that the larger mirror irregularity tolerances in parentheses are for the case where irregularity is dominated by astigmatism.

The advantage of this final specification is that it clearly differentiates the manufacturing procedures. The position tolerances are attainable on a conventional lower-cost precision machine (Makino A51), and the irregularity tolerances are achievable on the Moore 650 FG machine.

4.3 Opto-mechanical Design and Manufacturing/Assembly Procedure

Based on Table 4, after several iterations, the prototype system shown in Fig. 7 was designed. The frame and the mirrors are aluminum 6061T6. The mirror mounting uses three-ball three-vee kinematic mounts as in the previous design. Mirrors M1 and M3 have no adjustment and are therefore mounted in a monolithic piece as shown. The three-vee kinematic mount for mirror M2 is mounted on a commercially available precision mechanical stage is with x-y-z compensation. The mirror kinematic mounts are preloaded with stinger screws through the center that deform mechanical springs. The detector is mounted on a three-axis stage for defocus adjustment (s) and later to hold and move a spherical reflector for wavefront testing, where the x-y adjustment can then be used to move the spherical reflector to different points on the image plane.

This system is designed to be tested in the lab, not used in a service environment, so environmental requirements are not stringent. It was also made stiff enough to avoid issues with deflection and/or print through of the mirror light-weighting pattern onto the surface. However, it was desired to reduce the weight for portability by light-weighting. The mirrors and the metering structure were light-weighted with triangular pockets, as shown. The web thickness of the light-weighting cells is 3.175 mm, and their depth is 20 mm. Thus, the face sheet thickness of the mirror blanks is variable but is not less than 10 mm. The entire system has a mass less than 30 kg, and this mass could be significantly reduced by further light-weighting. For service situations, the frame design and the materials could be modified as needed with the same optical design.

The opto-mechanical system is designed to allow a manufacturing procedure that will meet or exceed and verify tolerances at each step. The procedure is as follows. All of the components are rough machined, including the mirrors to near net shape (i.e., freeform surfaces). A kinematic vee fixture suitable for all three mirrors is mounted to the spindle of the Moore 650 FG and indicated to a plane perpendicular to the spindle axis as described below. Each

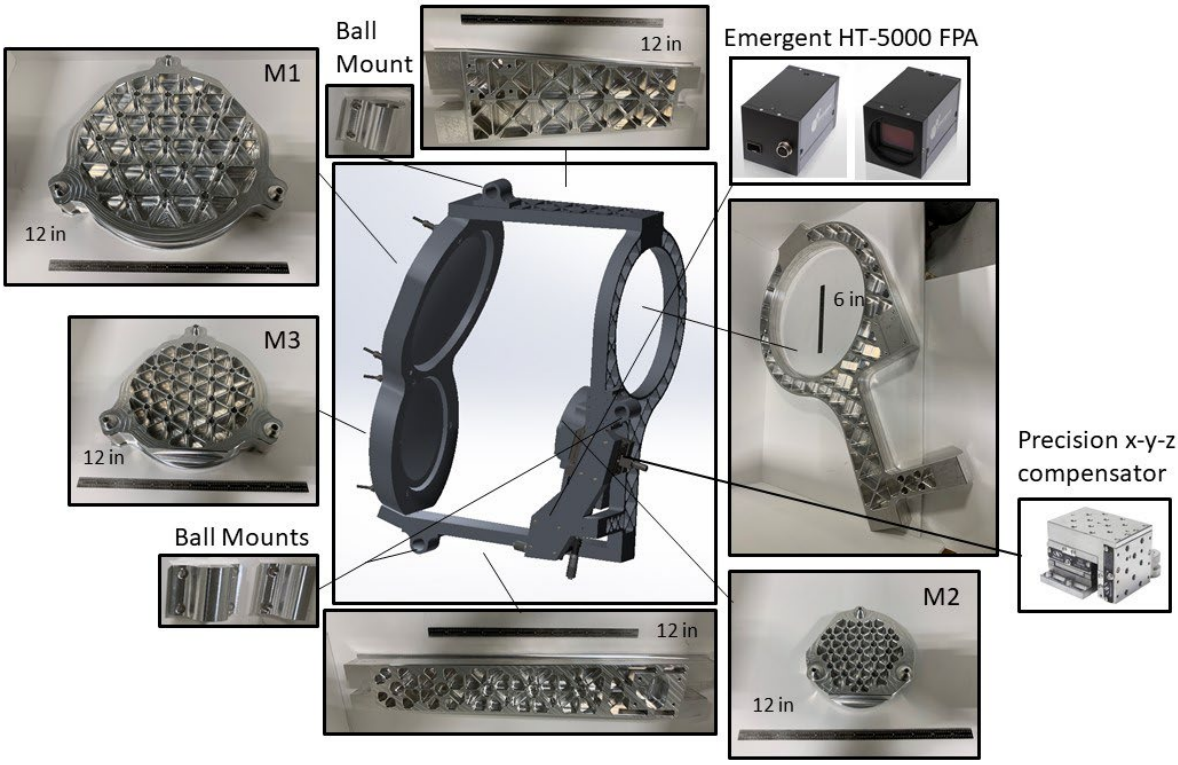

Fig 8. Manufactured and purchased components.

mirror is mounted to Moore 650 FG kinematically, and the freeform surfaces are machined and verified by on-machine metrology. The distance from the zero point on the optical prescriptions for the finally ultra-precision diamond tuned pass to the center of the kinematic balls is determined as described below. Next, the rough machined frame or metering structure (without the mirrors and the positioning stages) is assembled with three balls at its base. The structure is kinematically mounted to the Makino A51 machine, and the vees for M1 and M3 are machined at the correct locations to put the known mirror surfaces at the correct locations, based on the measurements of the zero points relative to the ball centers made on the Moore 650FG within the tolerances given in Table 4. In the same setup, a plane is machined to orient the base of the x-y-z precision stage for M2. Finally, the x-y-z precision stage for M2 and the adapter with the vee grooves for M2 are mounted on the structure. The structure is reoriented on the Makino A51, still using the kinematic mount, and the vee grooves for M2 are finish machined to ensure the angular orientation of M2 relative to M1 and M3. Finally, the mirrors are placed in the assembly on the Makino A51. Using the Makino A51 as a coordinate measuring machine, M2 is moved on the x-y-z precision positioning stage to its nominal position ± 2.5 micrometers. The stage can then be locked in position so that – as with the monolithic design – the mirrors can be quickly removed from and replaced in the structure as a "snap-together" design, and the frame/metering structure is not intended to be disassembled after final assembly. The only adjustment in this now "monolithic" system is the x-y-z compensation of M2 to recover optical performance. After assembly and nominal positioning of M2, the system is also ready for optical testing as outlined below. Most of the components have been rough manufactured or purchased, as shown in Fig.8.

4.4 Optical Surface Manufacturing

The most difficult part of the project, and the one where the tolerances are hardest to meet, is the machining of the freeform surfaces on the mirrors. All surfaces are being machined on the Moore 650 FG diamond machining center, and we will use mirror surface M2 as an example here. In its simplified form, the diamond machining of a freeform surface on a metal blank consists of the following steps: (a) centering of the diamond tool on the spindle axis and

determination of its actual radius by turning and measuring a test sphere and repeatedly making corrections, (b) mounting and alignment of the kinematic fixture on the spindle, (c) programming the machine to cut the freeform prescription (after numerous verification steps ensuring that the surface being fabricated meets the expectations of the optical designer), (d) cutting of the optical surface.

4.4.1 Tool Centering

Two main geometric corrections must be done on a tool prior to machining an optical surface – centering relative to the spindle axis and determining the tool radius at the sub-micrometer level. In two-axis diamond turning, it is well-known that decenter of the tool relative to the axis of rotation will cause characteristic form errors in the diamond turned spherical surface. Centering must be done in two directions (machine axes X and Y) to avoid these errors and center defects. For coordinated axis turning of freeform surfaces, it is particularly important to center first using a spherical artifact. Errors in the figure of a freeform surface due to tool decenter and radius errors can be extremely difficult to recognize in subsequent freeform metrology (if available) can be difficult to differentiate from other sources of error because they depend on the freeform prescription. They are even more difficult to recognize in subsequent optical testing when several surfaces and the associated errors are now producing a combined optical effect.

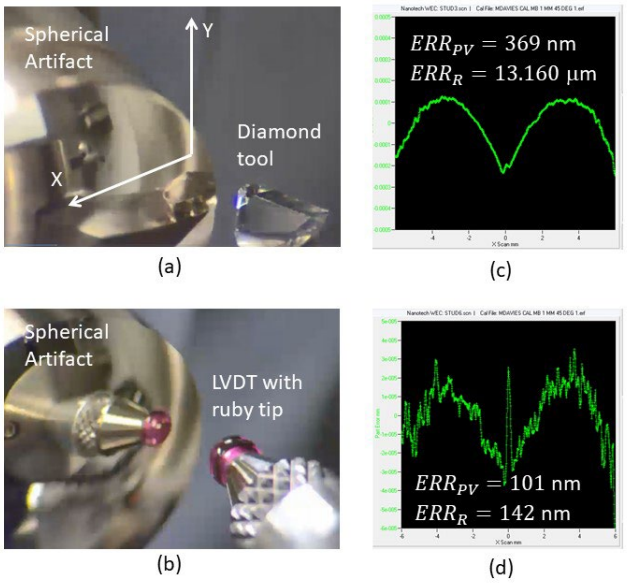

Fig 9. (a) Spherical test artifact, (b) LVDT measurement system, (c) error form when tool is not reaching the spindle center, (d) final error after adjustment.

The tools used in this work are 0.5 mm (nominal) radius, controlled waviness tools with zero-degree rake angle. The tools used for this project, the waviness certificates provided by the supplier show less than 20 nm of waviness. Control of the waviness is important because it is transferred to the surface directly as errors. Although we have corrected for waviness in research work [18], correcting it using commercial CAM software (NanoCAM4 is used for this work) is not currently possible.

Rough centering of the tool to sub-micrometer level is done with an on-machine microscope with associated software that recognizes the tool edge, fits it with a circle, finds the tool center and then gives the coordinate shifts required to put the tool on the center of rotation of the spindle. The microscope is kinematically connected to the machine, and its position will repeat to less than a micrometer, so that the shift to spindle center can be stored and re-used. However, this rough centering procedure is not sufficient to produce surfaces with the desired irregularity tolerances.

Fine centering is done by cutting and measuring the form error of a spherical artifact. As the tool moves over a surface, the cutting point moves around the tool edge, so the spherical artifact should "sample" at least as much of the tool edge as the surfaces to be cut. In this case, the freeform surfaces all have slopes that are less than 10°. The spherical test artifact had a radius of curvature of 12.7 mm and a clear aperture of 12.7 mm, so that 30° of the tool edge was required to cut the full sphere, meeting the criterion. A spherical artifact on the machine with the diamond tool approaching the surface is shown in Fig. 9 (a). Before centering in the horizontal (X) direction, the tool is first centered in the vertical direction (Y) by simply cutting the artifact and examining it in a microscope to identify the center defect. The tool center is adjusted in the Y direction until the center defect is no longer visible at 200x magnification.

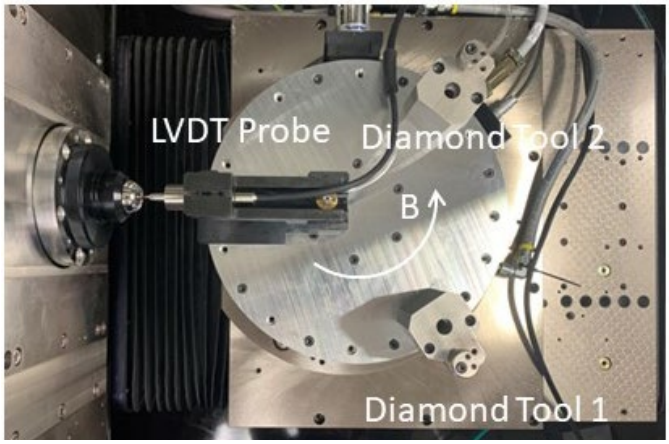

Fig 10. Two diamond tools and LVDT probe arranged on the rotary B axis of the Moore Nanotechnology 650 FG machine.

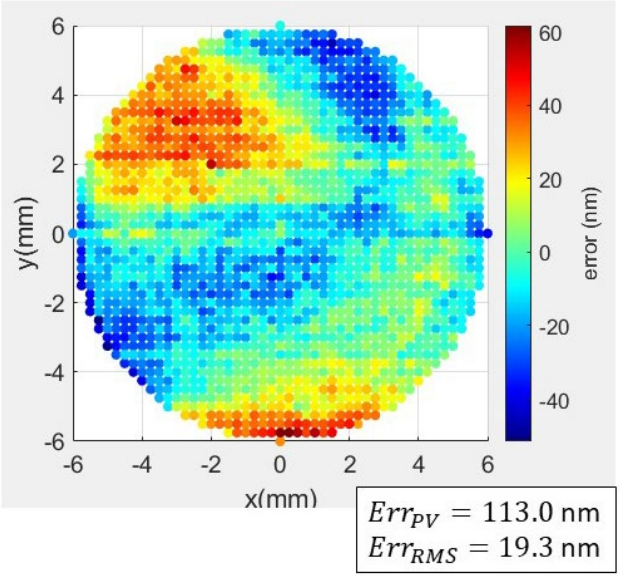

Fig 11. Three-dimensional error map of 12.7 mm test stud.

The centering in X can be determined by the deviation of the artifact from a perfect sphere. A measurement profile was done in this case with a controller-integrated linear variable differential transformer with a porous graphite air bearing to constrain a plunger that has a ruby ball at the tip (see Fig. 9(b)). Alternatively, the artifact may be removed from the machine and measured on a profilometer of sufficient accuracy. Alternatively, it can be measured on a noncontact device such as an interferometer (although the radius is not determined from this measurement). If the tool does not cut fully to the center, when the error is calculated by subtracting the best fit circle from the measured profile, then the errors will be negative at the center, become positive and then positive again (so-called "M" shaped error). Conversely, with the tool cuts past the center, the pattern reverses (so-called "W" shaped error). The decenter can be estimated from the peak-to-valley error magnitude and the error shape. For example, Fig. 9(c) shows the initial deviation from the circle of the cross section of an artifact cut with a tool that was initially centered with the microscope. The error is in the shape of an "M" and thus indicates that the tool is not cutting fully to the center of the artifact. The estimate of the additional distance needed to travel by the tool to reach the center was 3.4 μm, and a radius error of 13.16 μm is also identified. After correcting the X decenter, the artifact was re-machined twice, leading to a total X correction of 2.2 μm. A radius reduction of 0.278 μm was applied to the manufacturers reported radius of 515 μm. The final result is Fig. 9(b), which deviates from a circular cross-section by only 101 nm and in radius from the programmed 12.7 mm by only 142 nm. Two tools and the measurement LVDT were set up on the rotary B-axis of the machine, as shown in Fig. 10. This allowed for the use of two unworn tools and the LVDT probe to simultaneously cut and measure each optical surface.

While the LVDT probe is set up on the machine controller to measure only profiles for tool centering and/or correction of aspheres, we developed a procedure and program for three-dimensional metrology of freeform surfaces on the machine. Figure 11 shows a scan of the test stud made in less than an hour using the LVDT probe. The PV error of the entire sphere is only 113 nm PV and 19.3 nm RMS. Because the probe radius and the probe centering on the part is also critical for accurate measurements, measurements of the test stud were used to determine the probe radius 0.996 mm (1.000 mm nominal), and reversal techniques were used to center the probe on the spindle to less than 250 nm in X and Y. This scanning routine will be used to measure the freeform surface of M2 below.

4.4.2 Kinematic Fixture Mounting and Metrology

Prior to mounting the mirrors on the machine spindle, a kinematic, three-vee fixture was manufactured and mounted on the spindle. This fixture is able to accommodate the three mirror sizes. Because the mounting is kinematic (a) the

Fig 12. Mounting, measurement and adjustment of the kinematic fixture.

mirrors can be removed, measured on other equipment, and then returned to the Moore 650 FG for correction; and (b) the mirrors are being mounted for manufactured in the same fixturing condition and in the same orientation as they will be mounted in the final system. Thus, the effects of any mounting stresses (minimized for kinematic mounts already) and gravitational loads should be reduced.

Before the mirrors could be mounted on the machine, the fixture needed to be mounted on the spindle and centered. Also, deformations due to spindle mounting on the center bolt circle needed to be minimized so that the mirror tangent plane is parallel to the seats of the plane generated by the seating of the kinematic balls to within desired tilt tolerances (Table 4). To minimize the deformations, the fixture was mounted to the spindle with the center bolt pattern, and then three hardened steel cylinders were mounted in the position of each mirror with a measured seating moment of 17.5 N-cm. The Z-positions of each of the cylinder crests was then measured with the LVDT probe and the moments on the center bolt pattern were adjusted so that the Z-heights varied by less than 300 nm as shown in Fig 12. Over the 122 mm clear aperture of M2, the tilt is 2.46 μrad, an order of magnitude lower than the tolerances in Table 4. This procedure must be repeated to check and adjust the alignment for each mirror.

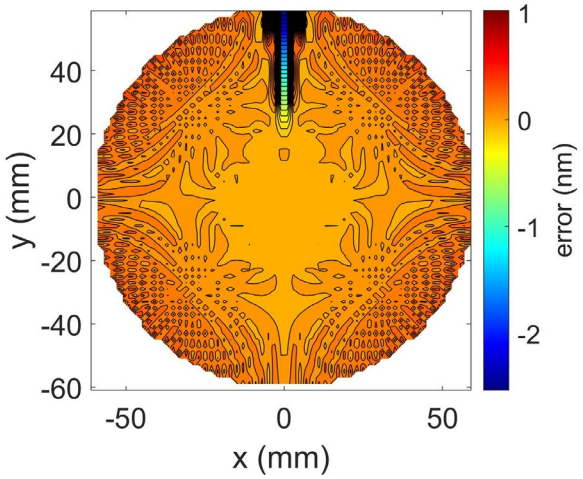

Fig 13. Errors of the tool path in comparison to analytical prescription.

4.4.3 Optical Surface Diamond Machining

Once the fixture was mounted and aligned, the mirror M2 was mounted on the fixture using the same seating moment (17.5 N-cm), and diamond machined. Programming of the machine motions was done in NanoCAM4/5, and the programmed tool paths were verified against the prescription in MATLAB. The errors of the programmed toolpath from the prescription for M2 are shown in Fig. 13. They are at the nanometer level and are due to the approximation made by the software to calculate the tool path (NURBs approximation). This is a necessary check as many CAM packages do not generate tool paths with enough fidelity to meet optical irregularity specifications.

After the tool path is generated and verified, the optical surface is cut with the diamond tool. Mirror M2 being cut (inset with red sharpie ink to indicate that surface is entirely machined) and as finished is shown in Fig. 14.

4.5 On-Machine Surface Metrology

After the surface was machined, it was measured using the on-machine LVDT probe and the custom software mentioned earlier. The measurement process for a freeform surface using a ball is not a trivial task. In order to

measure a specific grid of points on the surface, the center of the ruby ball must be commanded to move to certain locations and then to measure the Z-height of the surface at those positions. To measure a specified point on the surface (x,y, $z(x,y)$) the unit surface normal at each desired measurement point (x,y) must first be calculated from Eq. (2).

$$\hat{\boldsymbol{e}}_{\boldsymbol{n}} = \frac{\boldsymbol{\nabla F}}{|\boldsymbol{\nabla F}|} \tag{2}$$

Here the function $F(x,y,z)$ is a set of level curves defined as follows,

$$F(x,y,z) = z - f(x,y) = c \tag{3}$$

where the surface prescription is defined by $z - f(x,y)$ and c is a constant. Then the probe position is calculated for each desired surface point (x,y, $z(x,y)$) by offsetting the surface position by the probe radius R_P at each point so that the probe positions are given by Eq. (4).

$$\begin{aligned} x_P &= (\hat{\boldsymbol{e}}_{\boldsymbol{n}} \cdot \hat{\boldsymbol{e}}_{\boldsymbol{x}})R_P \\ y_P &= (\hat{\boldsymbol{e}}_{\boldsymbol{n}} \cdot \hat{\boldsymbol{e}}_{\boldsymbol{y}})R_P \\ z_P &= (\hat{\boldsymbol{e}}_{\boldsymbol{n}} \cdot \hat{\boldsymbol{e}}_{\boldsymbol{z}})R_P \end{aligned} \tag{4}$$

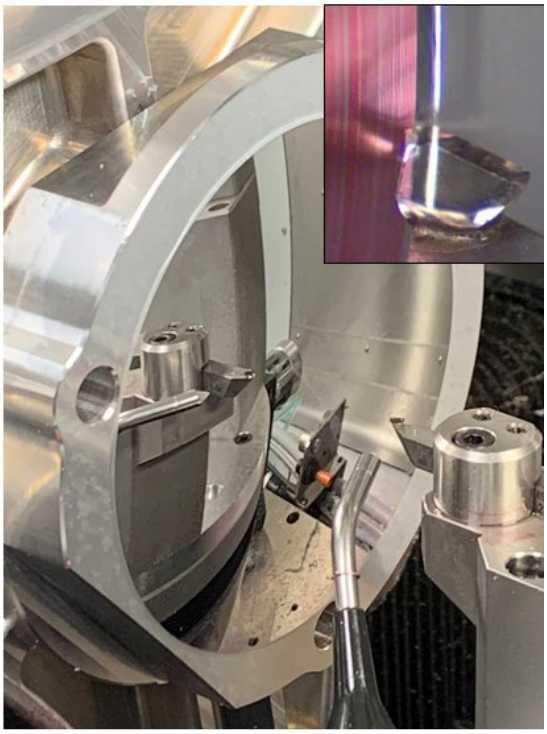

Fig 14. Machining of Mirror M2 freeform surface.

When the prescription is given in polar coordinates, the gradient must be calculated in polar coordinated and then transformed back to Cartesian coordinates. The probe is now programmed to move the points (x_P, y_P, z_P) and measure the actual position z_M. Finally, the measured points (x_P, y_P, z_M) must be transformed back to the surface using the *ideal* normal vectors. This approximation is a potential source of measurement errors. A MATLAB® program was written to do these calculations and generate the NC programs to control the machine and command it to make the measurements. While this method of measurement is common on coordinate measuring machines, this is the first implementation that we are aware of on a commercial diamond turning machine to measure freeform optics.

Mirror M2 was measured over a grid of points spaced by 2 mm in x and y. The errors between the measurements and the prescription are shown in Fig. 15(b). The errors were fit to 36 Zernike polynomials to determine the dominant terms and potentially to enter corrections into the NC code for machining. The results of the fit are shown in Fig. 15(b). The most dominant Fringe Zernike terms are Z_4(defocus), Z_5 and Z_6 (astigmatism), Z_7 and Z_8 (coma), Z_9 (trefoil) and Z_{11} (quadrafoil). Of these, the most dominant are Z_5, Z_6 and Z_9. Concerning the tolerance specifications in Table 4, the following conclusions can be drawn: (1) the irregularity is larger than the specification of 460 nm but smaller than the 920 nm allowed if dominated by astigmatism, (2) it remains unclear if the errors are actually on the optical surface as rotations of the part and remeasurement do not appear to cause a rotation of the dominant error pattern. Thus, it is suspected that they may be related to assumptions in the measurement procedure, and if so, then the actual surface errors are likely within the tolerance. If this is the case, correction of the surface manufacturing code may reduce the apparent errors but could lead to significant actual errors on the surface. Currently, we are working to determine the effect of these errors – if they are real – on the optical performance of the system. The answers to these questions will decide the future directions. We will also attempt independent metrology and assess its agreement of disagreement with the on-machine measurements.

5. CONCLUSIONS AND FUTURE WORK

Two three-mirror freeform imager configurations have been discussed. The first one-third scale (83 mm aperture) system was designed and built with a monolithic housing/metering structure. While the imaging performance revealed by wavefront error measurements is less than desired (1.25 μm of RMS wavefront error at the center of the focal

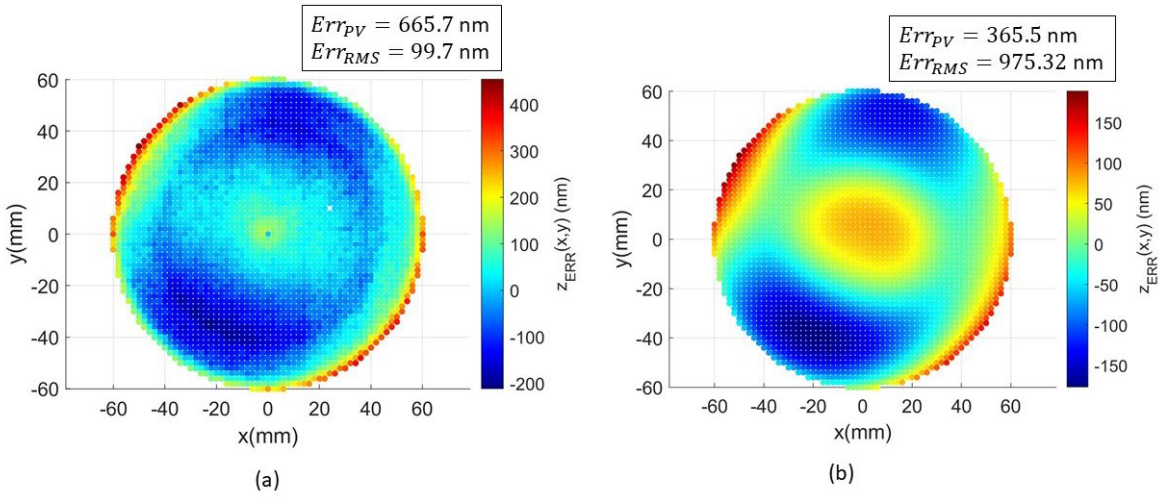

Fig 15. (a) Measured errors on mirror M2 and (b) 36 term Fringe Zernike polynomial fit to the errors.

plane) the wavefront repeatability was good (25 nm RMS wavefront variation on assembly/disassembly). This finding showed that the assembly method, using the three-ball, three-vee kinematic mounts is very repeatable as confirmed by subsequent research [9]. The cause of the large wavefront error was suspected to be mirror irregularity, but at the time the prototype was completed no on-machine or independent metrology systems were available for measuring the mirrors.

The second larger design (250 mm aperture) used a similar kinematic mounting system for mirror placement and assembly, and while the housing is assembled, final machining will be done after assembly, treating the housing/metering structure as a monolith. However, a commercial precision displacement stage was used to build-in adjustment of M2 in the assembled structure. In some sense this design is still "snap-together" because once the positon of M2 is set for optimal imaging, the system can still be disassembled and assembled rapidly. The introduction of three degrees of freedom on M2 allowed for much more attainable tolerances on mirror placement and irregularity. On-machine metrology was developed to "close the loop" on manufacturing, although independent metrology is still needed to confirm the measurement results.

Once the system is completed, it will be tested using an extended knife's edge technique as described by Reichenbach et al. [19]. Wavefront testing may also be done at the site of an industrial partner.

6. ACKNOWLEDGEMENTS

We gratefully acknowledge the National Science Foundation (NSF) I/UCRC Center for Freeform Optics (IIP-1338877, IIP-1338898, IIP-1822049, and IIP-1822026) and Industry members of the Center for Freeform Optics (https://centerfreeformoptics.org). Tom Nelson and Peter Marasco at the Air Force Research Laboratory provided substantial support and technical input. We also gratefully acknowledge support from the DURIP grant FA9550-19-1-0149 from the Air Force Office of Scientific Research and Dr. Stacy Williams at AFOSR.

7. REFERENCES

[1] K.P. Thompson, J.P. Rolland, Freeform optical surfaces: A revolution in imaging optical design. *Optics and Photonics News*, 23(6):30-35, 2021.

[2] W.T. Plummer, J. G. Baker, J. Van Tassell, Photographic optical systems with nonrotational aspheric surfaces," *Appl. Opt.*, 38, 3572–3592, 1999.

[3] P. J. Smilie, B. S. Dutterer, J.L. Lineberger, M. A. Davies, T. J. Suleski, Design and characterization of an infrared Alvarez Lens, *Optical Engineering*, 51(1), 013006, 2012.

[4] J.P. Rolland, M.A. Davies, T.J. Suleski, C.J. Evans, A. Bauer, J.C. Lambropoulos, K. Falaggis, Freeform optics for imaging, Optica 8, 161-176, 2021, https://doi.org/10.1364/AO.410350.
[5] A. Bauer, E. M. Schiesser, J.P. Rolland, Starting geometry creation and design method for freeform optics, *Nat. Commun.*, 9, 1756, 2018.
[6] N.W. Horvath, M.A. Davies, Concurrent engineering of a next generation freeform telescope: mechanical design and manufacture, *Proc. SPIE*, 10998: 140 – 147, 2019, https://doi.org/10.1117/12.2518954.
[7] T. Noste, C.J. Evans, J.A. Miller, L.E. Hopper, Concurrent engineering of a next-generation freeform telescope: metrology and test, *Proc. SPIE* 10998:148-156, 2019, https://doi.org/10.1117/12.2519162.
[8] N. W. Horvath, I. W. Barron, J. D. Owen, B. S. Dutterer, E. Schiesser, A. Bauer, J. P. Rolland, and M. A. Davies, Optomechanical design and fabrication of a snap together freeform TMA telescope, *Proc. ASPE 32nd Annual Meeting*, 133-138, 2017.
[9] N. Horvath, M. Davies, S. Patterson, Kinematic mirror mount design for ultra-precision manufacturing, metrology, and system level integration for high performance visible spectrum imaging systems, *Precision Engineering*, 60:535-546, https://doi.org/10.1016/j.precisioneng.2019.09.011.
[10] A. Bauer, E. M. Schiesser, J.P. Rolland, Analyzing the Aberration Fields of a Three-mirror Telescope and Correcting them Using Freeform Zernike Surfaces, *Optical Design and Fabrication 2017, OSA Technical Digest*, paper JW3C.4., 2017.
[11] C. J. Evans, Precision Engineering: An Evolutionary View (Cranfield Press, 1989).
[12] C. J. Evans, Precision engineering: an evolutionary perspective, *Philosophical Transactions of the Royal Society A: Mathematical, Physical and Engineering Sciences*, 370, 3835-3851 (2012).
[13] R. J. Benjamin, Diamond turning at a large optical manufacturer, *Optical Engineering*, 17, 574-577 (1978).
[14] T. Saito, Diamond turning of optics, *Optical Engineering* 15, 431-434 (1976).
[15] J. B. Bryan, Design and construction of an 84 inch diamond turning machine, *Precision Engineering*, 1, 13-17 (1979).
[16] R. Donaldson, and S. Patterson, Design and construction of a Large, vertical axis diamond turning machine, *Proc. SPIE*, 0433, 62-67 (1983).
[17] S. R. Patterson, and E. B. Magrab, "Design and testing of a fast tool servo for diamond turning," Precision Engineering 7, 123-128 (1985).
[18] J. D. Owen, J. A. Shultz, T. J. Suleski, M. A. Davies, Error correction methodology for ultra-precision three-axis milling of freeform optics (2017) CIRP Annals – Manufacturing Technology, 66(1):97-100. https://doi.org/10.1016/j.cirp.2017.04.031
[19] S. E. Reichenbach, S. K. Park, R. Narayanswamy. Characterizing Digital Image Acquisition Devices, *Optical Engineering*, 30.2: 170–177 (1991).